# H I Distribution and Kinematics of UGCA 86

J. M. Stil

*Department of Physics and Astronomy, University of Calgary*

*2500 University Drive NW, Calgary, AB, T2N 1N4, Canada*

stil@ras.ucalgary.ca

A. D. Gray

*Dominion Radio Astrophysical Observatory*

*Herzberg Institute of Astrophysics, National Research Council Canada*

*P. O. Box 248, Penticton, BC, V2A 6J9, Canada*

Andrew.Gray@nrc-cnrc.gc.ca

and

J. I. Harnett

*Faculty of Engineering, University of Technology, Sydney*

*P. O. Box 123, Broadway, NSW, 2007, Australia*

jules@eng.uts.edu.au

## ABSTRACT

We present 21-cm H I line and 408 MHz and 1.4 GHz continuum observations of the Magellanic dwarf galaxy UGCA 86, made with the DRAO synthesis telescope. UGCA 86 is detected in the continuum at both frequencies, with 408 MHz flux density $S_{408} = 120 \pm 30$ mJy and 1.4 GHz flux density $S_{1400} = 79 \pm 3$ mJy. The H I structure of UGCA 86 is complex, with two separate components: a rotating disk and a highly elongated spur that is kinematically disjunct from the disk. The H I disk is centered on the optical galaxy with similar axial ratio and orientation of the major axis. An area of the disk with a peculiar velocity of $\sim 25$ km s$^{-1}$ relative to the regular rotation of the disk is found on the southern side, where most of the star formation is concentrated. The spur is seen along the minor axis of UGCA 86 and overlaps in part with the disk. Towards the

optical center of UGCA 86, the velocity difference between the spur and the disk is 40 km s$^{-1}$, about one third of the rotation velocity of the H I disk at 6 kpc from the center. This implies a large radial component of the orbital velocity of the spur, and therefore a significantly non-circular orbit. The median H I velocity dispersion of the disk is 8.8 km s$^{-1}$, similar to other (dwarf) galaxies. The H I velocity dispersion of the spur varies from 10 km s$^{-1}$ to 30 km s$^{-1}$. A possible tidal origin of the spur is considered in view of the proximity of the large Scd galaxy IC 342. However, the orientation of the spur along the minor axis and its spatial overlap with the disk suggest that the spur is located far outside the plane of the H I disk. No evidence is found that the outer H I disk is warped, which poses a problem for the interpretation of the spur as a tidal tail induced by IC 342. Detailed modelling of the IC 342/UGCA 86 system will be required before a tidal origin of the spur can be dismissed conclusively. The possibility that the spur is part of the nascent cloud of UGCA 86 or the remains of a small dwarf galaxy is presented as an alternative interpretation.

*Subject headings:* galaxies: dwarf — galaxies: kinematics and dynamics — galaxies: structure – galaxies: individual (UGCA IC 342) — radio lines: galaxies — galaxies: ISM

## 1. Introduction

UGCA 86 is a Magellanic spiral (Sm) galaxy originally catalogued from optical plates by Nilson (1974). It is also known as A0355+66 (Kraan-Korteweg & Tammann 1979), and was discovered independently through its H I emission by Rots (1979), who referred to it as A0355. UGCA 86 was proposed as a member of the Local Group based on an analysis of a colour-magnitude diagram (Saha & Hoessel 1991), but photometry of the brightest stars place it at a distance of 2.6 Mpc, in the IC 342/Maffei Group (Karachentsev & Tikhonov 1993; Karachentsev et al. 1997). UGCA 86 is located 94′ southeast of the center of the Scd galaxy IC 342, implying a minimum separation of 71 kpc for the assumed distance of 2.6 Mpc. The adopted distance is somewhat less than the 3.3 Mpc distance of IC 342 (Saha, Claver, & Hoessel 2002), but in view of the uncertainties, UGCA 86 is likely a satellite of IC 342. Its present distance from IC 342 is at least 50% larger than the distance between the Milky Way and the Magellanic clouds.

Optical studies are complicated by the low Galactic latitude of this galaxy ($b \simeq +11°$). Hodge & Miller (1995) found reddening $E(B-V) = 0.59 \pm 0.23$ for H II regions in UGCA 86, with no evidence for significant extinction inside UGCA 86. Surface photometry in $V$ and $I$

by Buta & McCall (1999) shows a nearly exponential surface brightness profile with central surface brightness $\mu_{0,\mathrm{V}} = 20.14$ mag arcsec$^{-2}$ and integrated magnitudes $V_\mathrm{T} = 11.89 \pm 0.07$, $(V-I)_T = 1.49 \pm 0.1$. Applying a standard Galactic extinction curve, the absolute magnitude in the $V$ band corrected for extinction is $M_V = -17.0$ with an uncertainty of at least one magnitude. The extinction-corrected central surface brightness is $\mu_{0,\mathrm{V}} = 18.3$ mag arcsec$^{-2}$. The shape of the optical isophotes is elliptical with mean axial ratio $b/a = 0.80 \pm 0.02$ and major axis in P.A. $26\overset{\circ}{.}8 \pm 1\overset{\circ}{.}8$. The optical axial ratio implies an inclination $i = 38^\circ$ for an intrinsic axial ratio $(b/a)_0 = 0.2$.

Hodge & Miller (1995) detected numerous H II regions in UGCA 86 adding up to a total star formation rate of 0.014 $\mathrm{M}_\odot$ yr$^{-1}$. Most of the star formation is concentrated in three H II region complexes southeast and southwest of the center of UGCA 86. The most prominent star formation complex is the "cometary" component to the south east (see Figure 20 of Buta & McCall 1999). That component is catalogued as VIIZw 009, and is well resolved into stars. It was suggested to be a separate, disturbed galaxy by Saha & Hoessel (1991), but has since been shown to be a part of UGCA 86 (Richter et al. 1991; Karachentsev & Tikhonov 1993; Hodge & Miller 1995). Buta & McCall (1999) likened the cometary component to the 30 Doradus complex in the Large Magellanic Cloud. The metallicity of H II regions 81 and 101 in Hodge & Miller (1995) is $\log(O/H) = -4.2$, comparable to the Large Magellanic Cloud (Kurt & Dufour 1998). Both these H II regions are associated with the cometary knot southeast of the center of UGCA 86. Richter, Braun & Assendorp (1998) argued that the cometary component is a more recent burst of star formation than the central part of the galaxy, and speculated that it was triggered by infall of gas. Infrared work on this galaxy has concentrated on the prominent H II regions in the south-west regions of the galaxy, with similar conclusions (Braun, Richter, & Schulz 2000). An X-ray source is located near the core (ROSAT source 1RXP J035951+6708.6), and has been suggested as being a low-mass X-ray binary (Richter, Braun & Assendorp 1998).

Rots (1979) showed that UGCA 86 is rotating, with a perturbed velocity field, and identified it as a Magellanic dwarf irregular galaxy. His H I mass reduced to a distance of 2.6 Mpc is $1.2 \times 10^9$ $\mathrm{M}_\odot$. Rots (1979) reported a systemic velocity $v_\mathrm{sys} = 85 \pm 5$ km s$^{-1}$. Other authors found a significantly smaller value $v_\mathrm{sys} = 72$ km s$^{-1}$ (Fisher & Tully 1981) and $v_\mathrm{sys} = 67 \pm 4$ km s$^{-1}$ (Bottinelli et al. 1990). The Galactic coordinates of UGCA 86 are $(l, b) = (139\overset{\circ}{.}76, +10\overset{\circ}{.}65)$. At this longitude, positive velocities are forbidden by Galactic rotation. Confusion with foreground Galactic H I is not a problem at velocities exceeding 10 km s$^{-1}$. The systemic velocity of UGCA 86 close to the systemic velocity of IC 342 ($33 \pm 4$ km s$^{-1}$) (Bottinelli et al. 1990), which adds to the suspicion that UGCA 86 is a satellite of IC 342. Rots (1979) further suggested that UGCA 86 is tidally interacting with IC 342 as a means of explaining the perturbations in the velocity fields of both galaxies. A

suggestion by Newton (1980) that UGC 2826 might be the perturber for IC 342 has since been ruled out by the high radial velocity of that galaxy (Strauss et al. 1992).

Rots' low-resolution (10′, 22 km s$^{-1}$) H I results are the only published H I maps of UGCA 86 to date. To address this lack and investigate the possible link between UGCA 86 and IC 342, we have mapped the decimetre radio continuum and neutral hydrogen distribution of both galaxies with 1′ spatial and 5.2 km s$^{-1}$ velocity resolution, using the Synthesis Telescope at the Dominion Radio Astrophysical Observatory (DRAO).

## 2. Observations and Reduction

Data from a pointing centered on the optical disk of UGCA 86 were acquired simultaneously in the H I-line and in continuum bands at 1420 MHz and 408 MHz (wavelengths of 21 and 74 cm, respectively). Data were also collected for IC 342 in a separate but overlapping pointing (the 1420 MHz primary beam diameter of the DRAO array is 107′ to half power; at 408 MHz it is 332′). Analysis of the IC 342 field is deferred to another paper.

Twelve sets of spacings were used, giving baselines from 12.9 m to 604.3 m at 4.3 m intervals, and yielding sensitivity to spatial structures from 1′ to $\sim 1^\circ$ at 1.4 GHz (and about 3.5 times those values at 408 MHz). These data were collected during 2000 October–December. Some brief technical details of the observations and reduction are given in the following sections; refer to Landecker et al. (2000) for full details of the Synthesis Telescope. All images presented below have been corrected for primary beam attenuation.

### 2.1. Neutral-Hydrogen Spectral Data

H I line data were collected in 256 contiguous channels over a 4 MHz band, spanning 844 km s$^{-1}$ (3.3 km s$^{-1}$ per channel) with a velocity resolution of 5.2 km s$^{-1}$. The observation was centered at +31 km s$^{-1}$, the heliocentric velocity of IC 342; UGCA 86 is nominally at +67 km s$^{-1}$, which is well within the same band. Both right- and left-hand circular polarizations were recorded, with the two being averaged to make the final images, resulting in an rms noise per channel of 9.5 mJy beam$^{-1}$. To remove continuum sources, channels free from hydrogen emission and band-edge effects were selected from each end of data-cube and averaged together (120 such channels were used), then the result was subtracted from each channel image.

The spatial resolution achieved from uniformly-weighted visibilities was $49'' \times 54''$ at P.A. $-0.^\circ3$; the data presented in this paper have had a radial taper applied to increase the

brightness temperature sensitivity, and have a beam of $59'' \times 65''$ at P.A. $-0\overset{\circ}{.}6$. A spectral line cube tapered to $1'.4$ resolution was made to obtain a better signal to noise ratio for faint extended emission. The well-sampled aperture plane and inherent low signal-to-noise meant that it was not necessary to deconvolve the channel images (a standard practice at DRAO). Missing short spacings cause a mild negative bowl.

### 2.2. Continuum Data

The 1.4 GHz continuum system records full polarization data in four 7.5 MHz bands, pairs of which flank the spectrometer band. Data from the four bands were gridded separately onto a common aperture plane to make a single image in each of the four Stokes parameters. The synthesized beam at 1.4 GHz was the same as for the radially tapered H I data described above, and the rms noise was 0.25 mJy beam$^{-1}$. No significant linear or circular polarization was seen from UGCA 86.

The 408 MHz continuum system records data over a 3.5 MHz bandwidth, in right-hand circular polarization only. In the absence of circularly polarized signal, which is generally the case, this may be interpreted as Stokes $I$. At 408 MHz the tapered synthesized beam was $3'.3 \times 3'.8$ at P.A. $-3\overset{\circ}{.}5$, and the confusion-limited rms noise achieved was 4 mJy beam$^{-1}$.

The data were processed in DRAO's `MADR` package. The raw Stokes $I$ image at each frequency was deconvolved using CLEAN, and self-calibrated to remove artefacts arising from variations of amplitude and phase on short time-scales during the observation.

## 3. Results and Analysis

### 3.1. Neutral-Hydrogen Spectral-Line

Figure 1 shows the H I channel maps of UGCA 86 at positive velocities. Emission of UGCA 86 is blended with Galactic emission at velocities below $\sim+10$ km s$^{-1}$. The location of the brightest emission associated with UGCA 86 changes gradually with velocity in a way consistent with a rotating disk. At velocities beyond 50 km s$^{-1}$ the structure in the channel maps is more complex. In addition to the brighter component, a faint spur of emission extends towards the northwest.

Figures 2 and 3 show the H I column density and velocity field, respectively, for UGCA 86. These images were constructed from a cube in which the emission from UGCA 86 was manually identified in each channel image and selectively masked to exclude areas with no

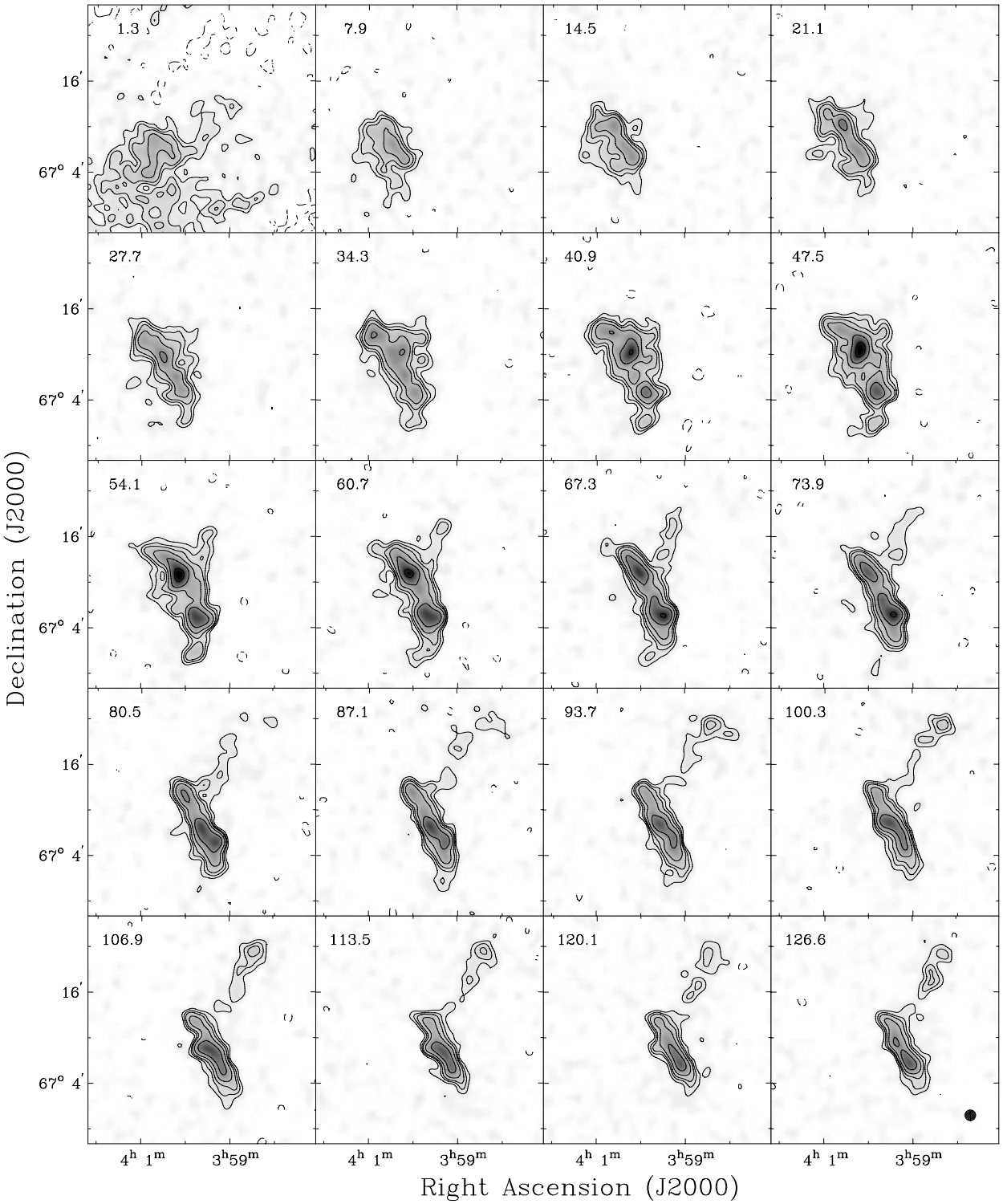


Fig. 1.— H I channel maps of UGCA 86 at 1.′4 resolution. Grayscales are linear from 0 mJy/beam (white) to 400 mJy/beam (black). Contours are drawn at −3, 3, 5, 7, 11, 19 and 35 times the r.m.s. noise per channel (9.5 mJy/beam). Velocities in km $s^{-1}$ are shown in the upper left corner of each panel. Channels near zero velocity are affected by Galactic foreground emission. The size of the synthesized beam is shown in the bottom right panel.

signal. In this way we minimized the adverse effects of noise in empty regions, and the contaminating Galactic H I emission at velocities below $\sim +10$ km s$^{-1}$. In these contaminated channels we also examined position-velocity slices though the data-cube to aid in the identification of emission from UGCA 86, which has higher velocity dispersion than the Galactic emission. The total H I mass of UGCA 86 derived from this masked dataset is $0.66 \times 10^9$ M$_\odot$. This is significantly smaller than the value found by Rots (1979). This difference cannot be attributed to resolution of the extended emission in Rots' map by the shortest baselines of the DRAO interferometer. The present data lack the sensitivity to detect the extended low column density emission in Rots' map, and the modest negative bowl has a negative effect on the flux when integrating over a large area. Differences in the treatment of confusing Galactic emission may also have contributed. Note that the extended emission in the first panel of Figure 1 is considered Galactic here.

The distribution of neutral hydrogen has a maximum column density of $2.5 \times 10^{21}$ cm$^{-2}$. The distribution is approximately elliptical in outline for column densities higher than $6 \times 10^{20}$ cm$^{-2}$ (Figure 2), with an extent of $13\farcm4 \times 9\farcm6$ at the $5 \times 10^{20}$ cm$^{-2}$ level, oriented at P.A. 50°. The axial ratio of H I column density contours in the range $4 \times 10^{20}$ cm$^{-2}$ to $8 \times 10^{20}$ cm$^{-2}$, excluding the spur, is $(b/a)_{\rm HI} = 0.72 \pm 0.02$. This part of UGCA 86 is centered on the optical galaxy with similar axial ratio and orientation of the apparent major axis (Rots 1979; Buta & McCall 1999). The velocity field in this area shows a well-defined rotational velocity gradient with the receding side of the galaxy in P.A. 287°. Both the hydrogen and optical disks are centered at ($\alpha_{\rm J2000}$, $\delta_{\rm J2000}$) = ($03^{\rm h}\,59^{\rm m}\,50\fs5$, $+67°\,08'\,37''$). There are three prominent "holes" in the H I at ($03^{\rm h}\,59^{\rm m}\,54\fs5$, $+67°\,07'\,37''$), ($04^{\rm h}\,00^{\rm m}\,04\fs5$, $+67°\,08'\,37''$), and ($04^{\rm h}\,00^{\rm m}\,28\fs5$, $+67°\,11'\,57''$), in which the column density drops below $4 \times 10^{20}$ cm$^{-2}$.

At low column densities the narrow H I spur noticed in Figure 1 extends towards the northwest (the approximate direction of IC 342), up to 12′ (9 kpc) from the center of UGCA 86. This structure is also visible in the low-resolution column density map of Rots (1979). A faint extension of the H I isophotes is seen on the opposite side of the disk near $04^{\rm h}\ 01^{\rm m}$, $+67°\ 04'$. The suggestion of an elongated structure that partially overlaps with the H I disk on the sky will be confirmed later by position-velocity diagrams and H I line profiles. The kinematics of the spur are ordered, with lower velocities occurring on the eastern side of the spur. Note that the velocity changes more rapidly along the minor axis of the spur than in the disk, and that the (apparent) velocity gradient has a different direction.

### *3.1.1. Rotation curve of the disk*

The velocity field (Figure 3) clearly shows the regular rotation of the disk. However, the spur affects the velocity field as it overlaps in position with the disk. The approaching side of the disk is also affected by confusion with Galactic H I. A tilted ring fit (Warner, Wright & Baldwin 1973) to the velocity field of Figure 3 was attempted to obtain the rotation curve of the disk. However, the results of the fit to the velocity field are skewed towards smaller rotation velocities because of the contaminating emission of the spur. This will be illustrated further in Section 3.1.2.

The best representation of the rotation curve of the disk was obtained by fitting the shape of the position-velocity diagram though the kinematic major axis of the disk. The P.A. of the kinematic major axis and an initial rotation curve were determined from the tilted ring fits. The rotation velocities of the annuli and the systemic velocity were adjusted manually to force the rotation curve to follow the bright curved ridge of emission in Figure 4. The resulting rotation curve is listed in Table 1. The total mass of UGCA 86 within the outermost radius of the rotation curve is $2.1 \times 10^{10}$ $M_\odot$.

The inclination of the H I disk is uncertain. The adopted inclination $i_{\rm HI} = 45°$ is based on the H I axial ratio $(b/a)_{\rm HI} = 0.72$ and an intrinsic axial ratio $(b/a)_0 = 0.2$. If the optical inclination $i_{\rm opt} = 38°$ is adopted, the velocities are 15% higher than listed in Table 1. The systemic velocity found here is consistent with the values of Fisher & Tully (1981) and Bottinelli et al. (1990), but significantly smaller than the 85 km s$^{-1}$ found by Rots (1979). This systematic difference may be the result of Rots discarding channels affected by Galactic emission, and inclusion of the spur.

A significant misalignment between the P.A. of the apparent major axis and the kinematic major axis is observed in UGCA 86. A small but significant misalignment between the kinematic and morphological major axis is not exceptional in dwarf galaxies. Skillman et al. (1988) interpreted a similar misalignment in the dwarf irregular galaxy Sex A as evidence that the gas in the disk describes non-circular orbits.

Figure 5 shows a position-velocity slice in P.A. 45°, approximately along the apparent major axis of the H I disk. A small area 3′.5 southwest of the center of UGCA 86 displays a significant departure from the regular rotation pattern of the disk. Locally the line of sight velocity deviates by 25 km s$^{-1}$ from the value expected from the rotation curve model of Table 1. The area where the velocity deviates more than 20 km s$^{-1}$ from the rotation model is indicated by the ellipse in the upper panel of Figure 5. The H I mass of this area integrated over the velocity range 40 km s$^{-1}$ to 90 km s$^{-1}$ is $2.9 \times 10^7$ $M_\odot$. Accounting for 30% helium by mass, the kinetic energy associated with this region is $2.4 \times 10^{53}$ ergs. This

energy is equivalent with the mechanical energy released by 240 supernovae.

### *3.1.2. Kinematics and mass of the spur*

Position-velocity slices parallel to the major axis (P.A. 322°) and the minor axis (P.A. 232°) of the spur are shown in Figure 6 and Figure 7 respectively. These slices were taken from the 1′.4 resolution cube to show faint emission in the spur. Galactic foreground H I is seen at negative velocities and close to zero.

The spur is clearly visible in the velocity range +50 km s$^{-1}$ to +140 km s$^{-1}$, far outside the velocity range permitted by Galactic rotation assuming circular orbits and a flat rotation curve. It is possible in principle that the spur is H I in the foreground that does not follow Galactic rotation. We note that the difference between heliocentric velocity and velocity with respect to the Local Standard of Rest (LSR) is only 2 km s$^{-1}$ for UGCA 86.

One possibility is that the spur is a high-velocity cloud (HVC) along the line of sight. The HVC complexes nearest to the line of sight are complex A and complex H in the velocity range $-80$ km s$^{-1}$ $> v_{LSR} > -210$ km s$^{-1}$ (Wakker & Van Woerden 1991). Association of the spur with these complexes is dismissed because of the large velocity difference. Instead, the spur could be considered a compact high-velocity cloud (CHVC), not associated with a large complex. However, the all-sky distribution of velocities of CHVCs in the LSR reference frame is dominated by the orbital velocity of the LSR around the Galactic center. The velocity of the LSR has a large component in the direction of UGCA 86, and no CHVCs with positive velocities in the LSR frame have been found in this part of the sky (De Heij, Braun & Burton 2002, and references therein). The probability that an extraordinary CHVC with a positive velocity is found in this location is very small. For this reason, the interpretation of the spur as a CHVC is rejected.

Lockman (2002) reported a population of H I clouds in the Galactic halo with velocities up to 50 km s$^{-1}$ beyond that allowed by Galactic rotation. Some of these clouds would be detectable in the present data (Lockman & Stil 2003). The spur is observed at much higher forbidden velocities. Also, the velocity gradient of the spur and the width of the H I line profile in the spur do not match the narrow line widths observed in these halo clouds (Lockman 2002, 2004).

A distinct velocity gradient is observed along both the major and the minor axes of the spur. This indicates that the actual velocity gradient is not aligned with either the major axis or the minor axis. The direction of the actual velocity gradient across the spur was determined by interactively changing the P.A. of position-velocity slices until no velocity gradient

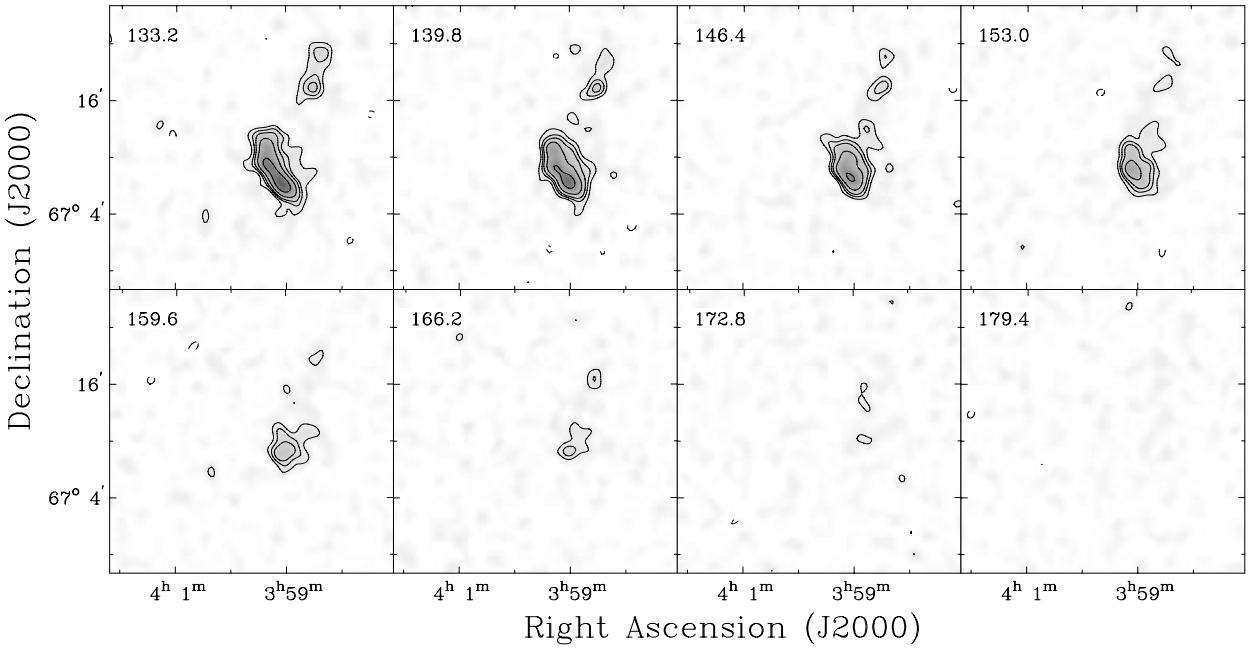


Fig. 1.— (continued).

Table 1. Rotation curve of UGCA 86

| radius ″ | Velocity km s$^{-1}$ | inclination ∘ | P.A. ∘ | $v_{\rm sys}$ km s$^{-1}$ |
|---|---|---|---|---|
| 60 | 35 ± 5 | 45 | 287 ± 2 | 72 ± 5 |
| 120 | 65 ± 5 | 45 | 287 ± 2 | 72 ± 5 |
| 180 | 87 ± 5 | 45 | 287 ± 2 | 72 ± 5 |
| 240 | 103 ± 5 | 45 | 287 ± 2 | 72 ± 5 |
| 300 | 114 ± 5 | 45 | 287 ± 2 | 72 ± 5 |
| 360 | 119 ± 5 | 45 | 287 ± 2 | 72 ± 5 |
| 420 | 122 ± 5 | 45 | 287 ± 2 | 72 ± 5 |
| 480 | 122 ± 5 | 45 | 287 ± 2 | 72 ± 5 |

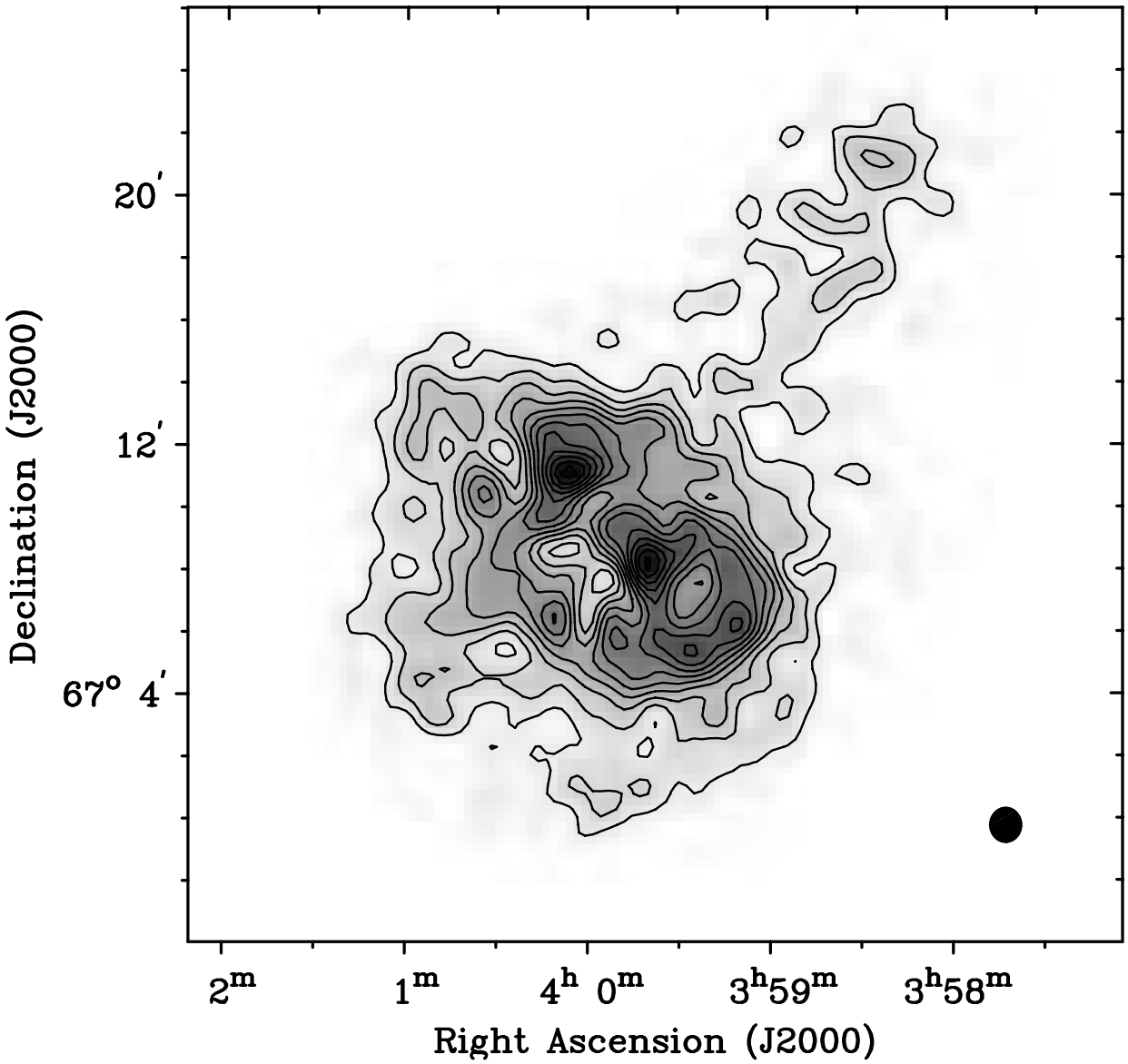


Fig. 2.— Contours of the H I column density for UGCA 86 superimposed on a grayscale of the same data. The contours are at $2 \times 10^{20}\,\mathrm{cm}^{-2}$ intervals starting at $2 \times 10^{20}\,\mathrm{cm}^{-2}$. The grayscale is linear from 0 to $2.5 \times 10^{21}\,\mathrm{cm}^{-2}$.

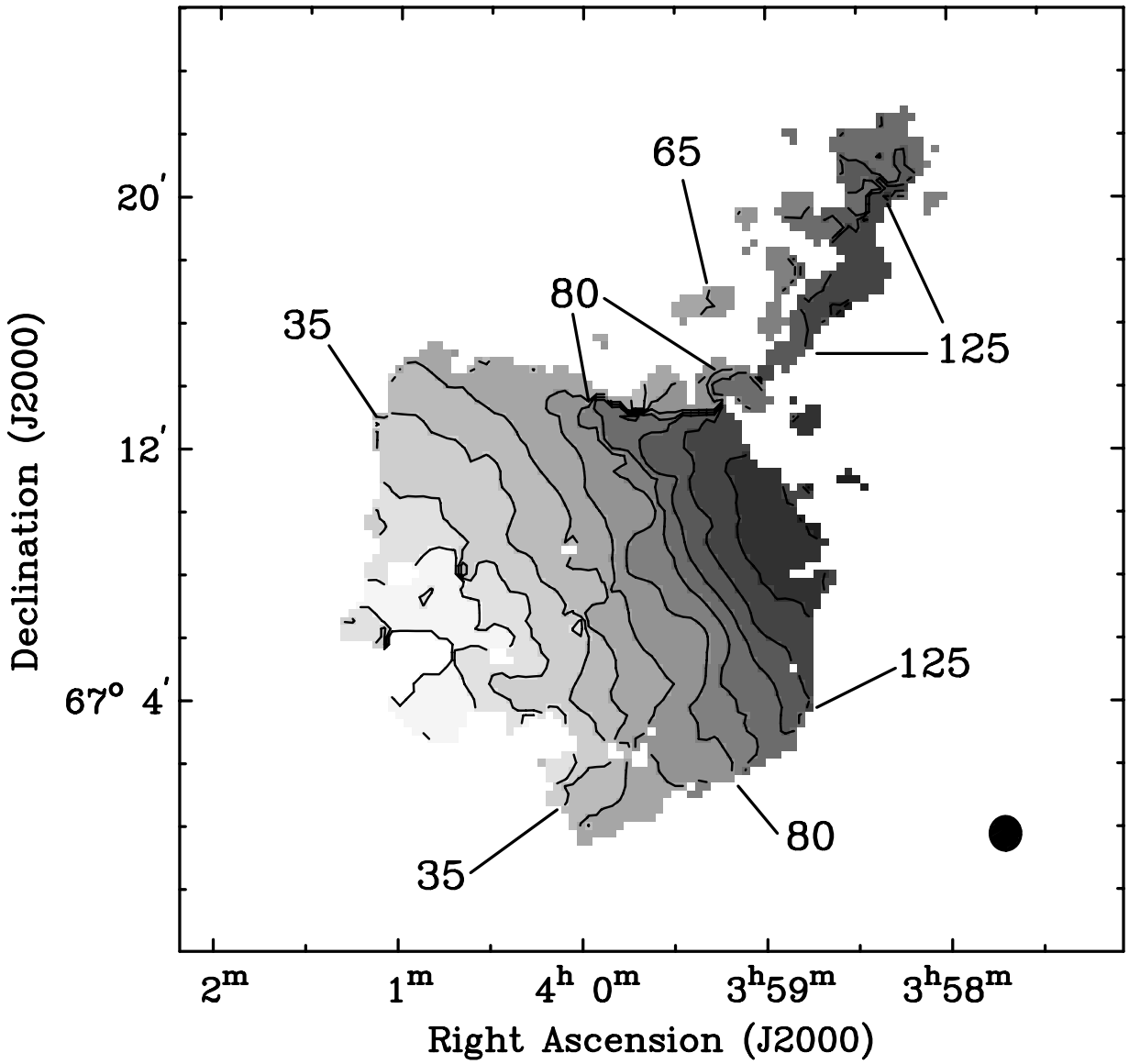


Fig. 3.— Contours of the velocity field for UGCA 86 overlaid on a grayscale image of the same data. The contours are at 15 km s$^{-1}$ intervals starting at −10 km s$^{-1}$. Selected contours are labeled with the corresponding velocity in km s$^{-1}$.

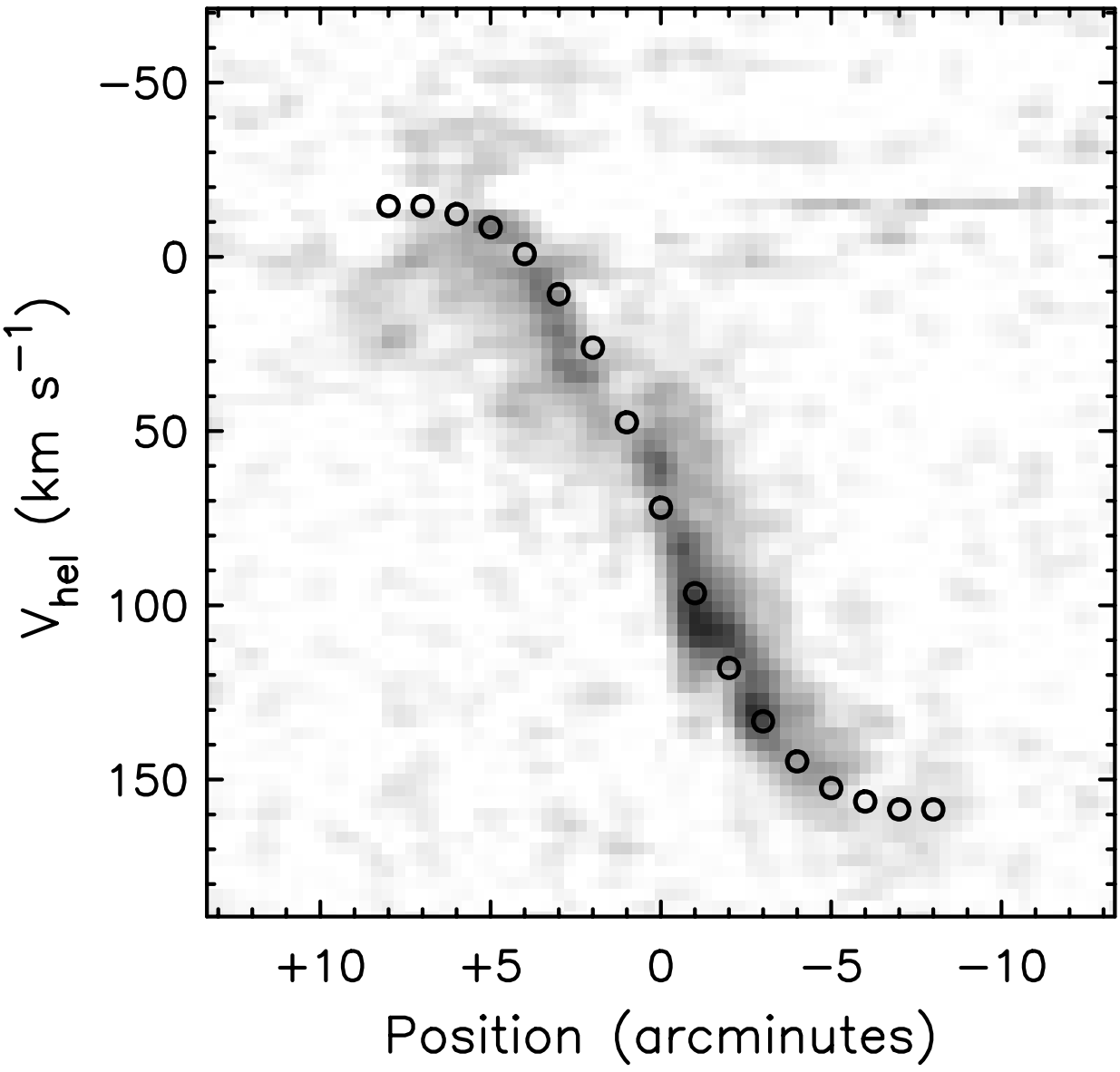


Fig. 4.— Rotation curve of UGCA 86, superimposed on a position-velocity slice along the dynamical major axis (position angle 287°). Position offset increases in the direction of right ascension. Grayscales are linear from 0 to 150 mJy/beam. Circles indicate velocities of the rotation curve listed in Table 1. Emission of the spur is also visible at velocities between 0 and $\sim +75$ km s$^{-1}$.

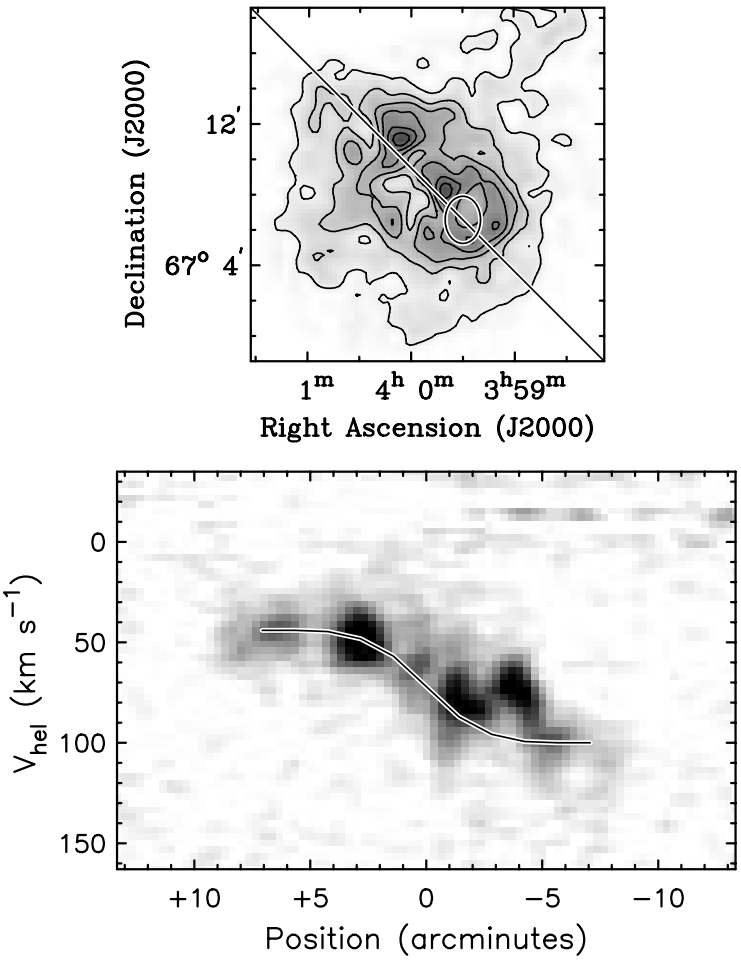


Fig. 5.— Position-velocity slice along the apparent major axis of UGCA 86. The top panel shows the location of the slice on the H I column density map. The ellipse indicates an area in the disk where the velocity deviates more than 20 km $s^{-1}$ from the line of sight velocity expected from the rotation curve and the inclination of the disk. The bottom panel shows the position-velocity slice. The curved line indicates the velocities calculated from the rotation curve in Table 1. Grayscales in the bottom panel are linear from 0 to 150 mJy/beam.

was discernible. This gives the P.A. of the direction perpendicular to the velocity gradient. The velocity gradient across the spur was found to be $\nabla v_{\rm spur} = 20.4$ km s$^{-1}$ arcmin$^{-1}$ in P.A. 75°. Evidence for a reversal of the velocity gradient is seen in slice D of Figure 6 towards the extreme end of the spur.

Figure 6 also shows that the spur does not begin at the northwest edge of the disk, but rather overlaps on the sky with the H I disk. The H I line profiles are double-peaked or blended where the spur and the disk overlap as illustrated in Figure 8. Double-peaked H I line profiles with a velocity separation of $\Delta v = 40$ km s$^{-1}$ are seen near the center of UGCA 86. Southeast of the center of UGCA 86 the line profiles are blended so much that a kinematic separation is not possible. The asymmetric line profiles on the southeast side do suggest that the spur extends across the disk. On the extreme east side of UGCA 86, the disk itself is difficult to disentangle from Galactic H I.

The difference $\Delta v$ in the line of sight velocity of the spur and the disk towards the center of UGCA 86 is a direct measurement of the velocity component of spur gas in the direction of the center of mass of UGCA 86, as defined by the optical galaxy. The radial component of the spur gas in this direction is a significant fraction, approximately one third, of the circular velocity at the last measured point of the rotation curve (Table 1). As the rotation curve appears to turn over around a radius of 300″, the velocity of a circular orbit at larger radii is not expected to exceed 122 km s$^{-1}$ by a significant amount. Therefore, the radial component of the velocity of this part of the spur is at least one third of the local circular velocity, independent of the actual distance from the center of UGCA 86. This significant radial component of the orbital velocity is a direct indication that the orbits of gas in the spur are significantly non-circular with respect to the center of UGCA 86.

A determination of the mass of the spur requires decomposition of the line profiles in a disk and a spur component in places where the spur and the disk overlap on the sky. Figure 8 shows that a decomposition of the line profiles into Gaussians will not provide a unique solution in many places. This ambiguity was addressed by subtracting a sequence of models for the H I disk from the data. These models were generated in three steps.

In the first step, a decomposition into at most two Gaussians was attempted at every location. The strongest Gaussian component was tentatively assigned to the disk. If no clear decomposition could be made, the profile was skipped in this step. In the second step, the central velocity of the Gaussian assigned to the disk was compared with the line of sight velocity expected from the rotation curve, the inclination of the disk, and the location in the disk. If the velocity difference exceeded a certain threshold, the fit was rejected. Thresholds of 0, 5, 10, 20 and 50 km s$^{-1}$ were applied to generate a sequence of disk models that assign less weight to the rotation curve and increasing weight to the Gaussian decomposition. In

the third step, rejected profiles and profiles that could not be decomposed into separate components in step 1, were replaced by a model Gaussian. This model Gaussian has a central velocity calculated from the rotation curve, amplitude equal to the observed intensity at the central velocity, and dispersion equal to the median velocity dispersion of the H I disk (13 km $s^{-1}$). Each model was subtracted from the data. The flux of the residual emssion was measured to obtain the mass of the spur. At this time, the anomalous velocity region shown in Figure 5 was masked out. It is not included in the mass of the spur. The H I mass of the spur was found to be in the range 4.8 $\times$ $10^7$ $M_\odot$ to 1.2 $\times$ $10^8$ $M_\odot$. The H I mass of the spur is approximately 10% of the H I mass of UGCA 86, but well within the range of H I masses of nearby dwarf galaxies (Karachentsev et al. 2004).

### *3.1.3.* H I *velocity dispersion*

The velocity dispersion of H I in the spur and the disk was determined by fitting a single Gaussian to the H I line profiles. The 1.′4 resolution data cube was regridded to 1.′5 pixels to obtain a single spectrum per beam. Line profiles with multiple components in places where the disk and the spur overlap were excluded from this analysis. Measurements of the velocity dispersion in the spur include areas west of $\alpha_{\rm J2000} = 3^{\rm h}59^{\rm m}$ and north of $\delta_{\rm J2000} = 67°16'$, which are separated spatially from the disk. Only 12 spatially independent profiles with sufficient signal were available in the spur. Some of the profiles in the spur appear to be the superposition of two or more components, but the limited signal to noise ratio does not warrant a decomposition into multiple Gaussians.

Figure 9 shows histograms of the H I velocity dispersion in the disk and in the spur. The median error for velocity dispersions is 1.0 km $s^{-1}$ in the disk, and 2.2 km $s^{-1}$ in the spur. The larger errors for the velocity dispersion in the spur are because of the generally lower brightness and the larger velocity dispersion.

The distribution of velocity dispersions in the disk is similar to that of other dwarf galaxies. The median velocity dispersion in the disk is 13.0 km $s^{-1}$, before corrections for spectral resolution and broadening by the rotational velocity gradient. Even though the number of measurements in the spur is small, Figure 9 indicates that the distributions of velocity dispersion differ between the spur and the disk. The median velocity dispersion in the spur is 19.4 km $s^{-1}$. Hunter, Van Woerden, & Gallagher (1999) found similar velocity dispersions in the outer cloud complexes of NGC 4449.

The line of sight velocity dispersions shown in Figure 9 have not been corrected for spectral resolution or for a contribution of the rotational velocity gradient. The correction

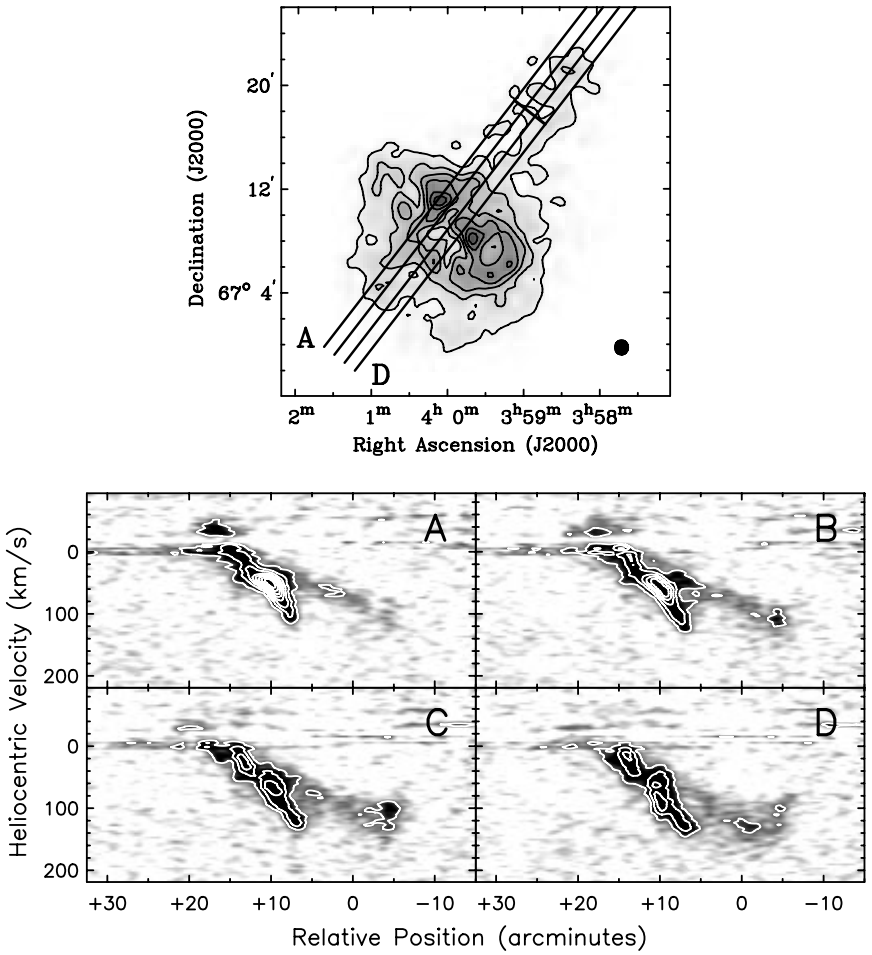


Fig. 6.— Position velocity slices along the major axis of the spur (P.A. 322°) extracted from the 1.′4 resolution cube. The location of the slices is shown on the H I column density map of Figure 2. Slices A and D are labeled. The short line perpendicular to the slices connects the locations of the zero points in the position-velocity diagrams. This line corresponds with slice C in Figure 7. Position offsets increase in the direction of Right Ascension. Grayscales in the position-velocity diagrams are linear from 0 (white) to 75 mJy beam$^{-1}$ (black). Contours are drawn at 50, 100, 150, ... mJy/beam.

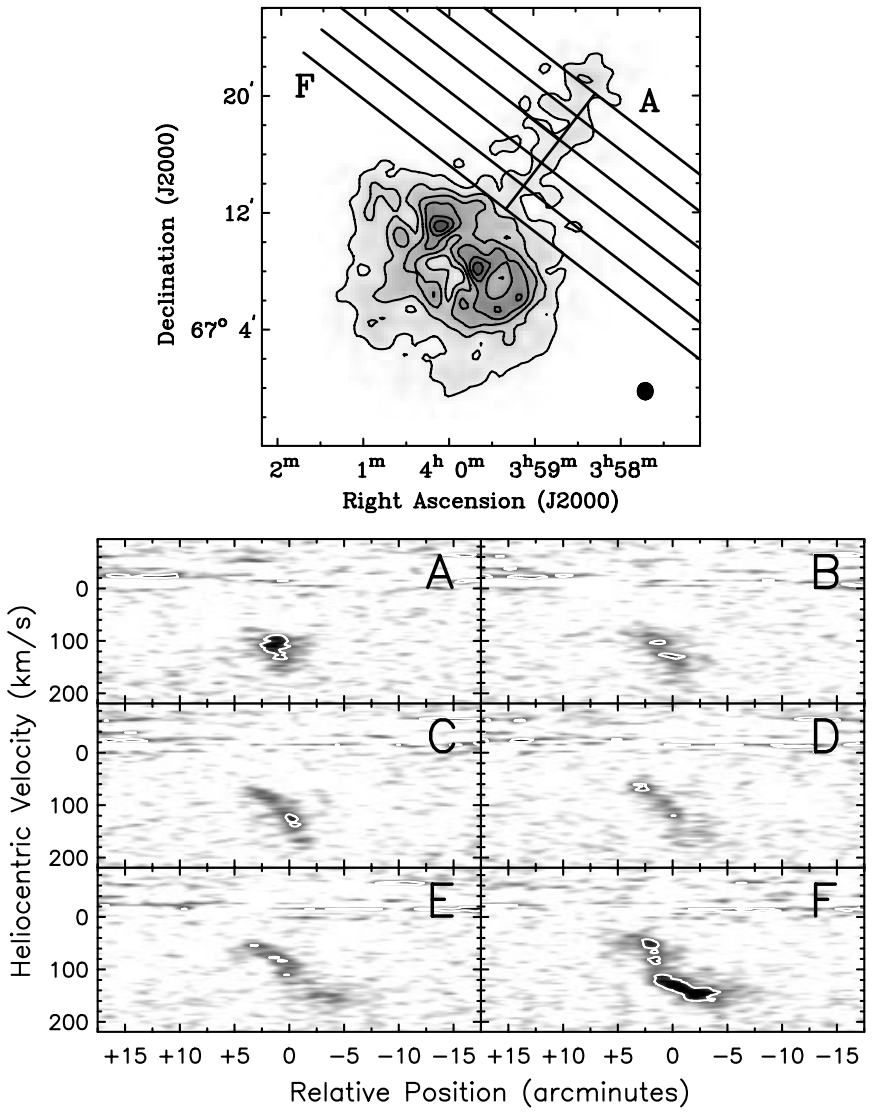


Fig. 7.— Position velocity slices along the minor axis of the spur (P.A. 232°) extracted from the 1′.4 resolution cube. The location of the slices is shown on the H I column density map of Figure 2. Slices A and F are labeled. The short line perpendicular to the slices connects the locations of the zero points in the position-velocity diagrams. This line corresponds with slice D in Figure 6. Position offsets increase in the direction of Right Ascension. Grayscales are linear from 0 (white) to 75 mJy/beam (black). Contours are drawn at 50, 100, 150, ... mJy/beam. The brightest emission in slice F is a part of the H I disk.

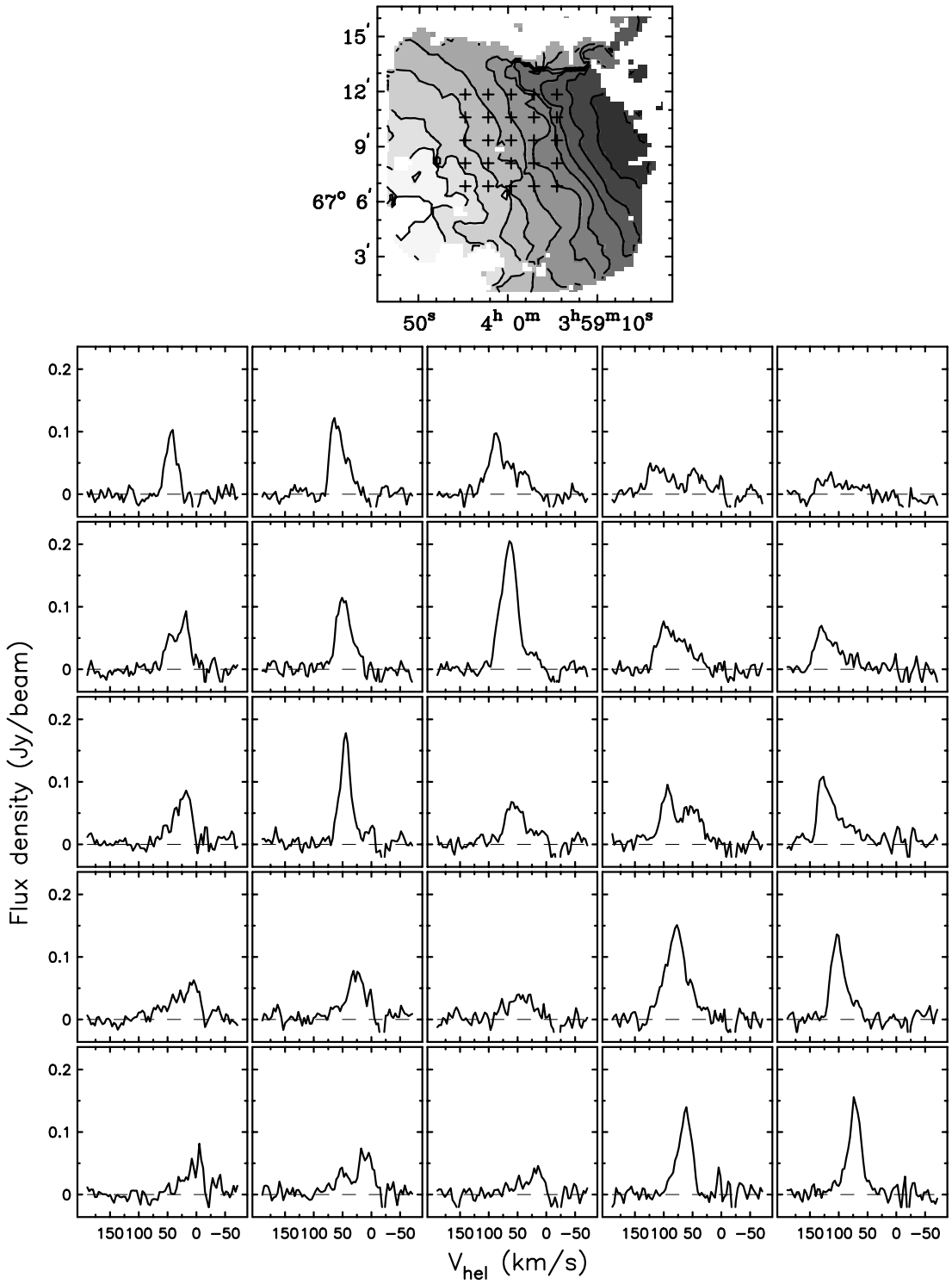


Fig. 8.— H I line profiles extracted from the 1′ resolution H I cube in the area where the spur and the disk overlap. Positions of the profiles are shown as + on the velocity field of Figure 3. The line profiles in the central area show two components separated in velocity by approximately 40 km $s^{-1}$. The least redshifted component is usually associated with the spur (see also Figure 6).

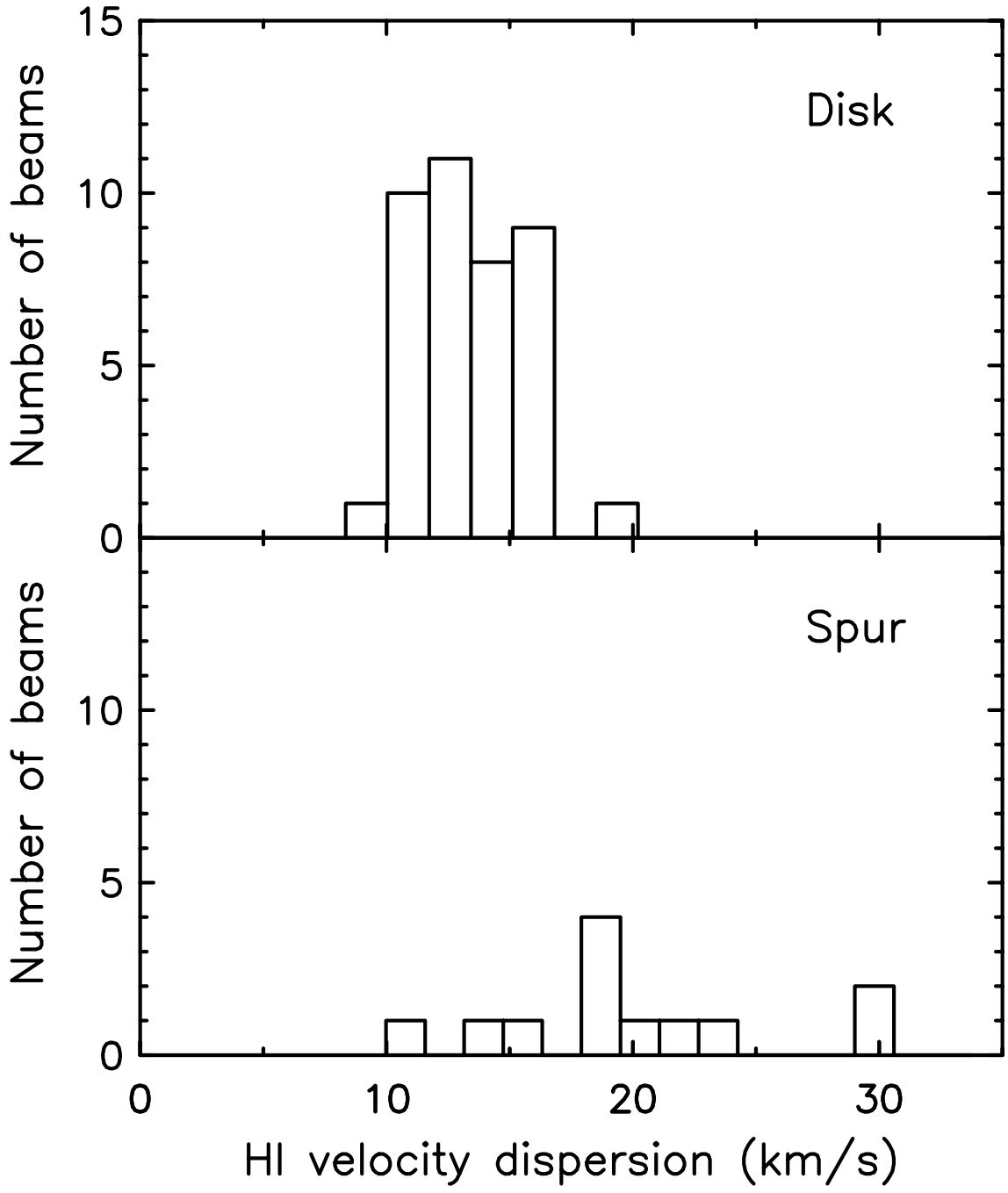


Fig. 9.— Distribution of the H I line-of-sight velocity dispersion in the disk of UGCA 86 (top) and in the H I spur (bottom).

for rotational broadening of the line profiles was done following Stil & Israel (2002b). The velocity gradient due to rotation of the disk derived from the rotation curve is $\nabla v_{\rm disk} = 13.6$ km s$^{-1}$ arcmin$^{-1}$. The instrumental spectral resolution is 5.2 km s$^{-1}$. The median velocity dispersion $\sigma = 13.0$ km s$^{-1}$ then results in a corrected line of sight velocity dispersion and spectral resolution $\sigma_{\rm HI} = 8.8$ km s$^{-1}$.

The velocity gradient across the spur contributes to the observed line of sight velocity dispersion in a similar way. For the velocity gradient $\nabla v_{\rm spur} = 20.4$ km s$^{-1}$ arcmin$^{-1}$, observed velocity dispersions of 15 km s$^{-1}$, 20 km s$^{-1}$, and 30 km s$^{-1}$ imply intrinsic velocity dispersions of 7, 15, and 27 km s$^{-1}$ respectively. The velocity gradient over the beam contributes to the high velocity dispersion observed in the spur, but its effect is too small to explain the difference in the distributions of the velocity dispersion in Figure 9. Adopting a single velocity gradient for the spur is a simplification. The smallest velocity dispersion measured in the spur is smaller than the broadening implied by the mean gradient. A more detailed analysis requires observations with higher spatial resolution.

### 3.2. Continuum emission

The 1.4 GHz radio continuum emission from UGCA 86 (Figure 10) shows a lop-sided distribution, with several emission peaks to the south and west of the optical center, embedded in an extended component that covers the entire optical disk. The strongest 1.4 GHz continuum emission coincides with the optical cometary component, and has a similar morphology. Emission peaks to the west and south-west of the optical center coincide with optical H II region complexes (Hodge & Miller 1995; Kingsburgh & McCall 1998) that are also seen in reprocessed IRAS data (Braun, Richter, & Schulz 2000). The H II region complexes appear on the periphery of depressions in H I column density. Two unresolved sources to the east have no optical or infrared counterparts, and are presumably background sources. The northern one is catalogued as NVSS J040022+670830 (Condon et al. 1998). No radio counterpart to the ROSAT X-ray source 1RXP J035951+6708.6 is evident.

UGCA 86 is also detected at 408 MHz. Three independent complete synthesis observations with UGCA 86 near the pointing center were analysed. One was centered on UGCA 86, one on IC 342, and one unrelated observation was available in the DRAO archive. UGCA 86 was detected in each of these 408 MHz observations. The 408 MHz image in Figure 10 is the linear mosaic of these three observations.

The total flux density at 1.4 GHz is $S_{1.4} = 79 \pm 3$ mJy, and at 408 MHz is $S_{0.408} = 120 \pm 30$ mJy beam$^{-1}$. The implied spectral index of UGCA 86 between 408 MHz and 1.4

GHz is $\alpha = -0.34^{+0.27}_{-0.20}$ ($S_\nu \propto \nu^\alpha$). While this is consistent with a nearly flat spectrum, it is likely that not all of the emission is thermal. The association of the compact emission with H II regions suggests that the the extended emission seen in the 21-cm continuum image may be significantly non-thermal. This is reminiscent of the extended synchrotron halo of the post-starburst dwarf galaxy NGC 1569, which has the same global spectral index $\alpha = -0.36$ (Israel & De Bruyn 1988). Extended synchrotron haloes are a rare phenomenon in dwarf galaxies. UGCA 86 is a prime candidate dwarf galaxy with a synchrotron halo.

## 4. Discussion

UGCA 86 is a member of a heterogeneous set of dwarf galaxies with very significant departures from ordered rotation in their extended H I envelopes. These galaxies are of interest for our understanding of the formation and evolution of galaxies because of the origin of the chaotic kinematics. We distinguish three broad categories that arguably share some common characteristics: 1. tidal interaction with another galaxy; 2. collision with or capture of an intergalactic H I cloud; 3. assembly of the H I disk on timescales longer than a Hubble time ("continuing galaxy formation" (Hunter et al. 1998)).

In case of tidal interaction, the H I displaying the peculiar kinematics is in fact the disturbed outer H I disk. The most extreme case of tidal interaction is a merger with another galaxy. In the case of a collision or capture of an intergalactic gas cloud or a smaller dwarf galaxy, the gravitational force on UGCA 86 may be negligible, but the infalling material may create large holes in the gas distribution and compress the interstellar medium to high densities in some places, triggering star formation (Tenorio-Tagle et al. 1986, 1987). The case of ongoing galaxy formation assumes that the H I was always bound to the dwarf galaxy, but has not yet been assimilated into the disk. An interesting question is why most dwarf galaxies do appear to have formed an H I disk, or even converted all of the available gas into stars. The main difference between a collision and ongoing assimilation is the time scale of the process. Both may be characterized as infall.

The relative importance of these processes is not well known. The number of (dwarf) galaxies with chaotic kinematics in their outer parts and the details of their kinematics provide important clues regarding the relative importance of these processes. This may in turn provide insight in similar processes occurring in galaxies at high redshift.

Although the orbits of the gas are not uniquely constrained by the observations, some constraints may be given if a geometry is specified. An important observation is the steep velocity gradient along the minor axis of the spur observed in Figure 7. This velocity gradient

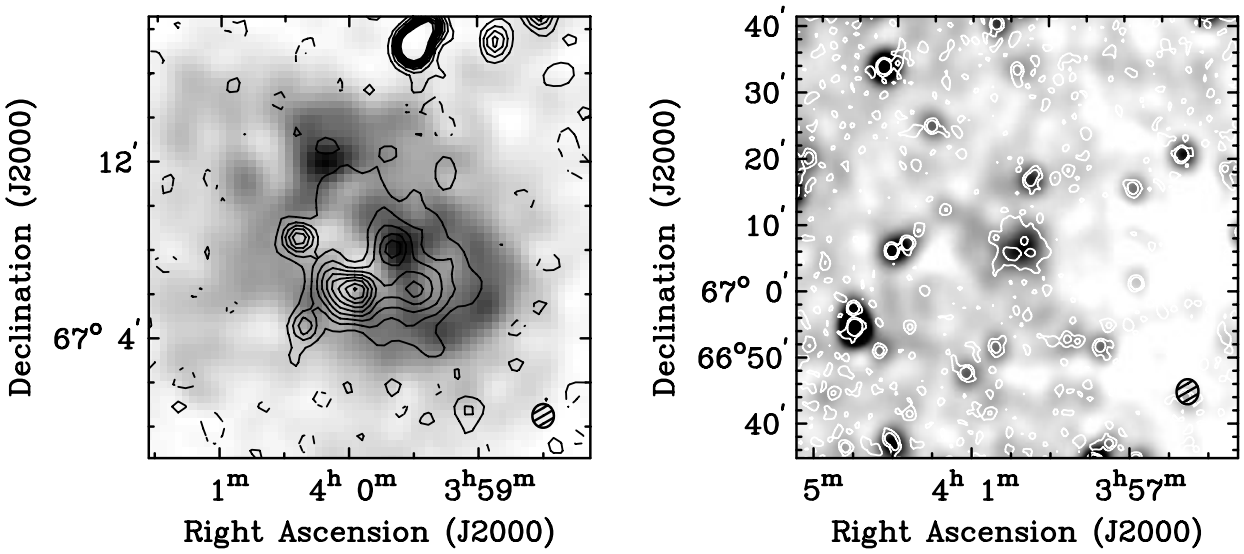


Fig. 10.— Contours of the 1.4 GHz continuum emission from UGCA 86 superimposed on (left) the H I column density grayscale (linear from 0 to $2.5 \times 10^{21}$ cm$^{-2}$), and (right) the 408 MHz continuum grayscale (linear from -6 to 60 mJy/beam) with a wider field of view. The black solid contours start at 0.5 mJy/beam ($2\sigma$), in steps of 0.75 mJy/beam. The dashed contour is at $-0.5$ mJy/beam. The white contours on the right indicate the 0.25 and 3 mJy/beam level in the 1.4 GHz continuum image. The hatched ellipses indicate the beam size of the 1.4 GHz continuum map (left) and the 408 MHz map (right).

is difficult to explain if the the spur is a filament, with its dimension along the line of sight equal to its minor axis on the sky. It would require a special short-lived geometry, or a mass concentration in the spur to balance the velocity shear and maintain its filamentary structure. It is more likely that the velocity gradient across the spur displays the line of sight component of the orbital velocity of gas in a structure that is extended along the line of sight. This argument is equally valid whether the orbits of the spur gas are open or closed. The large range in the H I velocity dispersion of the spur (Figure 9) is also most easily explained in terms of a superposition of multiple velocity components along the line of sight. Much of the following discussion is based on this argument.

### 4.1. Is the spur a part of the disk?

The H I velocity field around the optical galaxy shows the structure expected for a disk with well-ordered rotation. The first question that comes to mind is whether the spur is an extension of the H I disk of UGCA 86. The outer H I disk may not show well-ordered rotation as a result of tidal interaction with IC 342, or because it has not had the time to settle into a disk. However, if the spur is to be considered an extension of the disk, the orbits of H I in the spur should be reasonably circular around the optical galaxy and approximately in the plane of the observed H I disk. It should be noted that some dwarf galaxies appear to have significant warps in their outer H I disks, suggested by their twisted H I isophotes and a change in P.A. of the velocity field. Examples are DDO 168 (Broeils 1992; Stil & Israel 2002a,b), UM 439 (Van Zee et al. 1998), and NGC 4449 (Bajaja, Huchtmeier, & Klein 1994; Hunter et al. 1998).

Three lines of argument indicate that the gas in the spur does not satisfy these requirements. First, the spur partially overlaps in position on the sky with the H I disk, but not in velocity. This implies that at least this part of the spur is significantly out of the plane of the disk, because the orbits of gas in the spur cannot cross the orbits of gas in the disk. The second argument follows from the difference in the line of sight velocity between the spur and the disk in the direction of the optical center of UGCA 86. Although the rotation curve analysis of the velocity field did not uniquely define the position of the center of mass of UGCA 86, it is reasonable to assume that the center of mass is close to the optical center, as it is for larger disk galaxies. The correspondence between the morphology of the optical and the H I isophotes supports this assumption. The velocity difference $\Delta v$ is therefore the radial component of the orbital velocity of gas in the spur, with respect to the dynamical center of UGCA 86. For UGCA 86, $\Delta v \approx 40$ km s$^{-1}$ is about one third of the circular velocity of the outer disk at radius $8'$ (6 kpc). This large radial velocity component relative

to the local circular velocity implies that the orbit is significantly non-circular.

The first and second arguments combined imply that the part of the spur that is observed in the direction of the optical center is probably further from the dynamic center than the observed radius of the H I disk ($R_{\rm disk} = 6$ kpc). The distance of this part of the spur from the plane of the disk is then at least $R_{\rm disk}\cos(i) = 3.9$ kpc for the adopted inclination $i = 50°$.

The third argument that the spur is not an extension of the H I disk is that differential rotation would wind-up the spur on an orbital time scale $2\pi R_{\rm disk}/v_{\rm c} \sim 3 \times 10^8$ yr. The linear appearance of the spur would be highly coincidental because it would exist only for a short time.

The conclusion is that the H I spur is not an extension of the H I disk. This also excludes the possibility that the spur is an H I spiral arm similar to those observed in the extended outer H I disks of some dwarf galaxies, such as NGC 2915 (Meurer et al. 1996) and DDO 47 (Walter & Brinks 2001; Stil & Israel 2002a). At least some H I in the spur is found to follow non-circular orbits at a high inclination with respect to the plane of the H I disk. UGCA 86 is not unique in this respect. Highly structured outer H I with kinematics different from a disk that coincides with the optical galaxy has been reported for NGC 4449 (Hunter et al. 1998; Hunter, Van Woerden, & Gallagher 1999), IZw 18 (Van Zee et al. 1998), IIZw 40 (Van Zee, Skillman, & Salzer 1998) and NGC 1569 (Stil & Israel 1998, 2002c). IIZw 40 is a clear example of a merger in progress. The H I filaments in NGC 4449 may be the result of tidal interaction. However, Van Zee et al. (1998) suggested that the extended H I in IZw 18 is a remnant of the nascent cloud from which the galaxy formed. There is no known companion of NGC 1569 that could have caused the disturbed kinematics in its outer regions through tidal interaction. These examples show that there may not be a single origin of the disturbed H I kinematics in these systems. It is not possible in general to decide unambiguously which process occurs from H I observations of a particular galaxy.

### 4.2. The spur as a tidal tail

The proximity of IC 342 suggests that the spur may be the result of tidal interaction with this much larger neighbor. If the spur is a tidal tail induced by IC 342, some inferences can be made based on the kinematics and morphology of the spur. First, the velocity of the spur in the direction of the center of UGCA 86 is blue shifted relative to the H I disk. A tidal tail is expected to have a radial velocity component away from the center. This implies that the blue shifted spur gas should be located in front of the H I disk. Second, the 3-dimensional space velocity of the gas in a tidal tail is expected to vary smoothly with

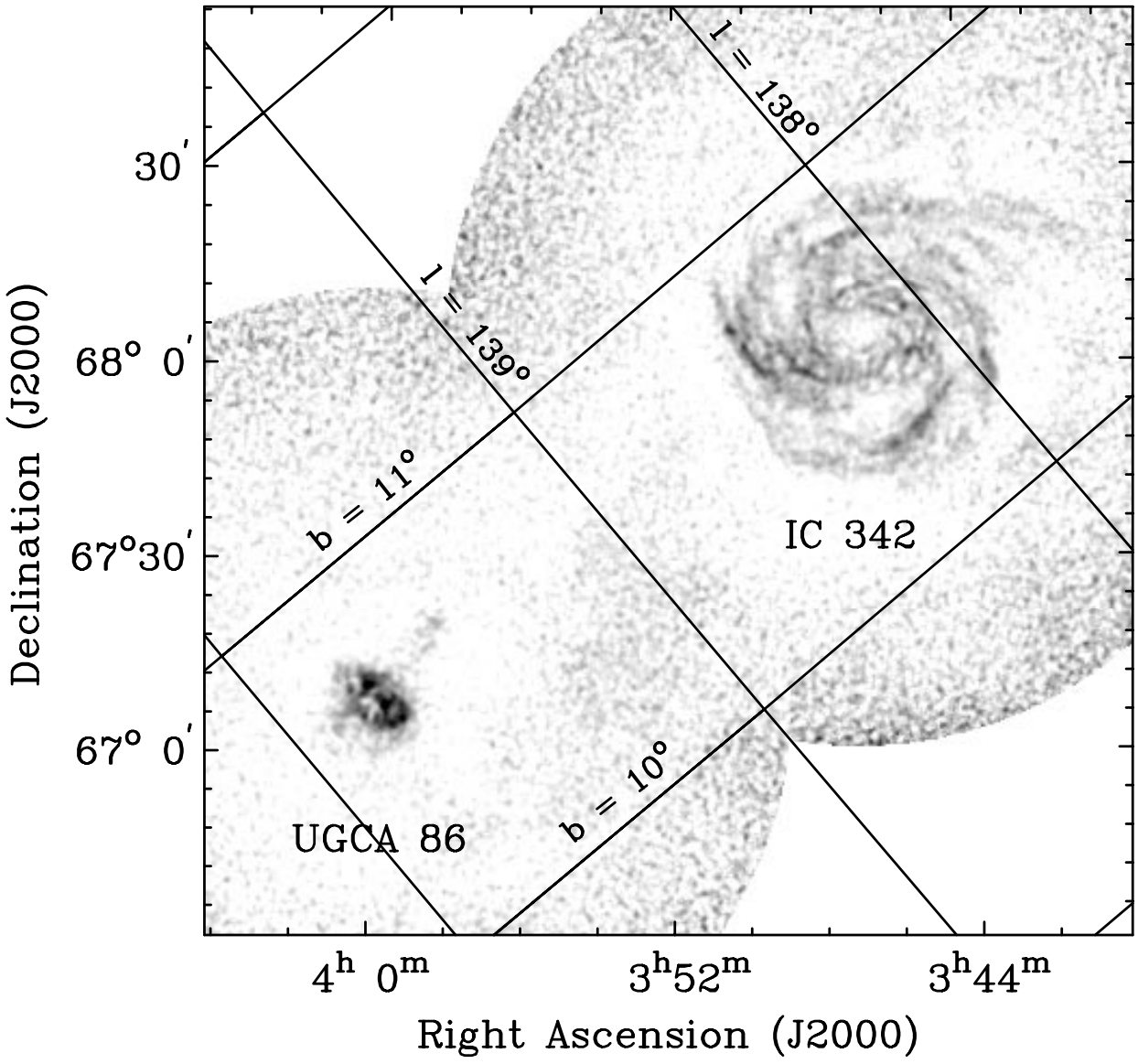


Fig. 11.— Mosaic of our two DRAO observations of the pair IC 342 and UGCA 86 showing the size and orientation of the spur in relation to the size and mutual distance of this pair of galaxies. The H I column density is shown in grayscales, linearly from $2 \times 10^{20}$ cm$^{-2}$ to $2 \times 10^{21}$ cm$^{-2}$. At a distance of 2.6 Mpc, 1 degree corresponds with 45 kpc. The faint extended emission between UGCA 86 and IC 342 is Galactic H I.

position along the tidal tail because adjacent test particles in the tidal tail always experienced similar accelerations during the interaction. This continuity of the spacial velocity should be seen in the data as a smooth gradient of the line of sight velocity along the tidal tail. The observed variation of the line of sight velocity along the *minor* axis of the spur is not necessarily in conflict with this expectation. The minor-axis velocity gradient may be the result of a projection effect where different parts of the tidal tail are seen close together on the plane of the sky. For this to be the case, the tidal tail must be in a plane that is observed nearly edge-on. The orientation of the spur along the minor axis of the optical and H I isophotes of the disk of UGCA 86 further means that the plane of the tidal tail makes a large angle (close to 90°) with the plane of the disk, no matter what the inclination of the disk might be. Third, the fact that the spur extends on the sky in the direction of IC 342, and the necessity that the spur is in a plane observed nearly edge-on, mean that IC 342 must be close to the plane of the spur. Fourth, if different parts of the tidal tail are to be seen in projection on the sky along the entire spur, the tip of the spur that appears most distant from UGCA 86 is a point where the line of sight is approximately a tangent to the tidal tail. If this is the case, one would expect that the spur is brighter at this point and that the velocity gradient along the minor axis vanishes. This expectation is confirmed by Figure 7.

The inference that IC 342 is in the same plane as the tidal tail is an interesting argument in favor of an interpretation of the spur as a tidal tail induced by IC 342. However, significant problems exist with this interpretation. If the spur is a tidal tail in a nearly polar plane, significant warping of the outer H I disk of UGCA 86 is also expected to occur. This warp should manifest itself by a change in P.A. of the H I isophotes and the velocity field of the disk. No such variation in P.A. is observed in Figure 2 and Figure 3. Van Zee et al. (1998) similarly argued that the component H I-SX in IZw 18 is not a tidal tail because of lack of continuity in the velocity field between the components H I-A and H I-SX. The necessity of a tidal tail in a plane that is perpendicular to the plane of the disk is by itself a problem because low-inclination encounters seem to be most effective in the formation of tidal tails (Toomre & Toomre 1972). Finally, in the inferred geometry the tidal tail appears in the direction of IC 342, with no evidence for a counter tail. This is contrary to simulations of tidally interacting disk galaxies, where the counter tail is the most prominent tidal feature (Toomre & Toomre 1972; Barnes 1988). Detailed modeling specific to this system is required to make these arguments conclusive.

### 4.3. The spur as a trigger of star formation

UGCA 86 currently experiences a period of enhanced star formation. The detection of UGCA 86 in the radio continuum, especially at 408 MHz, indicate exceptional star forming activity for a dwarf galaxy. Further evidence for significant recent star formation is seen in the numerous H II regions and the cometary knot.

It is tempting to associate the spur with the current star formation in UGCA 86. Gas falling into the disk as suggested by Richter et al. (1991) and Braun, Richter, & Schulz (2000) may have triggered the recent episode of star formation. Indirect evidence that this may have occurred is found in the region with anomalous velocity shown in Figure 5. This region occurs on the side of UGCA 86 that displays the most intense star formation. If the kinetic energy of this region is supplied by stellar winds and supernovae, the equivalent of more than 200 supernova explosions is required. The integrated star formation rate of UGCA 86 of 0.014 $M_\odot$ implies a supernova rate of $1 \times 10^{-4}$ supernovae per year for the entire galaxy, assuming a Salpeter IMF with low mass cut-off 0.01 $M_\odot$ and high-mass cut-off 100 $M_\odot$. The main H II regions are found on the periphery of the anomalous velocity region, not near the center. The power and the location of the star formation regions suggest that the observable population of high-mass stars is not the source of the anomalous velocity region. The impact of high-velocity clouds in a galactic disk has been suggested as an alternative energy source for super shells with very high energy requirements (Tenorio-Tagle et al. 1986, 1987). The presence of the spur and a kinematically disturbed region in the disk that requires more energy input than the observable stars can provide, lends some credibility to the suggestion of gas falling into UGCA 86.

## 5. Conclusions

We present H I, and 1.4 GHz and 408 MHz continuum observations of the Magellanic dwarf irregular galaxy UGCA 86 with the DRAO interferometer. The H I morphology of UGCA 86 is characterized by a rotating disk with inclination $\sim 50°$, but a significant misalignment exists between the optical/H I major axis and the kinematic major axis. In addition to this, a narrow spur of H I extends to the northwest, up to $12'$ (9 kpc) from the center of UGCA 86. The spur is oriented along the apparent minor axis of the disk of UGCA 86, and its kinematics are significantly different from the disk. The spur partially overlaps with the disk on the sky. The velocity difference between the spur and the disk towards the center of UGCA 86 is $\Delta v \approx 40$ km s$^{-1}$. In this direction we measure directly the radial component of the orbital velocity of gas in the spur. This large radial component, one third of the circular velocity at the edge of the H I disk, is evidence that the orbits of

gas in the spur are significantly non-circular. Also, the overlap of the spur and the disk on the sky, and the modest inclination of the disk imply that part of the spur is located well outside the plane of the disk, but no evidence for a warp of the outer H I disk is found. A well-defined velocity gradient is observed along both the major and the minor axes of the spur.

The mean H I velocity dispersion of the disk $\sigma_{\rm HI} = 8.8$ km s$^{-1}$ is similar to what is observed in other (dwarf) galaxies. However, the velocity dispersion of H I in the spur shows a large range, from 10 km s$^{-1}$ to 30 km s$^{-1}$.

UGCA 86 is also detected in the continuum at 1.4 GHz and 408 MHz. The 1.4 GHz continuum image shows the three largest H II region complexes, and an extended component that covers the entire optical disk of UGCA 86. At 408 MHz, the galaxy is unresolved. The global spectral index between 408 MHz and 1.4 GHz is $\alpha = -0.34^{+0.27}_{-0.20}$ ($S_\nu \propto \nu^\alpha$).

The interpretation of the spur as a tidal tail induced by IC 342, following an earlier suggestion by Rots (1979) is considered. In order to explain the observed H I kinematics of the spur, the tidal tail must be in a plane that is nearly perpendicular to the disk, although no warping of the outer H I disk is observed. Also, the spur is oriented in the direction of IC 342, which means that the prominent tidal tail is located in between the two interacting galaxies. Detailed modeling of the interaction between IC 342 and UGCA 86 is necessary to address these objections against a tidal tail interpretation of the spur.

If the spur is not a tidal tail, it is likely gas in an extended, non-circular orbit around UGCA 86. This gas may then be a remnant of the from the formation of UGCA 86 that has not yet settled into the disk, or an unlucky small dwarf galaxy that was tidally disrupted by UGCA 86.

## Acknowledgements

The Dominion Radio Astrophysical Observatory is operated as a national facility by the National Research Council of Canada. This research made use of the NASA/IPAC Extragalactic database (NED), which is operated by the Jet Propulsion Laboratory at Caltech, under contract with the National Aeronautics and Space Administration. JMS is grateful to dr. A. R. Taylor for financial support during this work. The authors thank dr. H. Lee for his comments on the manuscript.

## REFERENCES

Bajaja, E., Huchtmeier, W. K., & Klein, U. 1994, A&A, 285, 385

Barnes, J. E. 1988, ApJ, 331, 699

Bottinelli, L., Gouguenheim, L., Fouqué, P., & Paturel, G. 1990, A&AS, 82, 391

Broeils, A. 1992, PhD thesis, University of Groningen, The Netherlands

Braun, M., Richter, G. M., & Schulz, B. 2000, in ISO Beyond Point Sources: Studies of Extended Infrared Emission, eds. R. J. Laureijs, K. Leech, & M. F. Kessler (ESA Publications Division), p.155

Buta, R. J., & McCall, M. L. 1999, ApJS, 124, 33

Condon, J. J., Cotton, W. D., Greisen, E. W., Yin, Q. F., Perley, R. A., Taylor, G. B., & Broderick, J. J. 1998, AJ, 115, 1693

De Heij, V., Braun, R., & Burton, W. B. 2002, A&A, 392, 417

Fisher, J. R., & Tully, R. B. 1981, ApJS, 47, 139

Hodge, P., & Miller, B. W. 1995, ApJ, 451, 176

Hunter, D. A., Wilcots, E. M., Van Woerden, H., & Gallagher, J. S. 1998, ApJ, 495, L47

Hunter, D. A., Van Woerden, H., & Gallagher, J. S. 1999, AJ, 118, 2184

Israel, F. P., & De Bruyn, A. G. 1988, A&A, 198, 109

Karachentsev, I. D., & Tikhonov, N. A. 1993, A&AS, 100, 227

Karachentsev, I. D., Drozdovsky, I., Kajsin, S., Takalo, L. O., Heinamaki, P., & Valtonen, M. 1997, A&AS, 124, 559

Karachentsev, I. D., Karachentseva, V. E., Huchtmeier, W. K., & Makarov, D. I. 2004, AJ, 127, 2031

Kingsburgh, R. L., & McCall, M. L. 1998, AJ, 116, 2246

Kraan-Korteweg, R. C., & Tammann, G. A. 1979, AN, 300, 181

Kurt, C. M., & Dufour, R. J., 1998, Rev. Mex. A. A. Ser. Conf., 7, 202

Landecker, T. L., Dewdney, P. E., Burgess, T. A., Gray, A. D., Higgs, L. A., Hoffmann, A. P., Hovey, G. J., Karpa, D. R., Lacey, J. D., Prowse, N., Purton, C. R., Roger, R. S., Willis, A. G., Wyslouzil, W., Routledge, D., Vaneldik, J. F. 2000, A&AS, 145, 509

Lockman, F. J. 2002, ApJ, 580, L47

Lockman, F. J., & Stil, J. M. 2003, in Milky Way Surveys: The Structure and Evolution of Our Galaxy", eds. D. Clemens and T. Brainerd, ASP Conf Ser. `astro-ph/0310762`

Lockman, F. J. 2004, IAU Symp., 217, 130

Meurer, G. R., Carignan, C., Beaulieu, S. F., & Freeman, K. C. 1996, AJ, 111, 1551

Newton, K. 1980, MNRAS, 191, 169

Nilson, P. 1974, Uppsala Astron. Obs. Rep. No. 5

Richter, G. M., Braun, M., & Assendorp, R. 1998, in Highlights of Astronomy Vol. 11B, ed. J. Anderson (Kluwer Academic Publishers), p.101

Richter, G. M., Schmidt, K.-H., Thänert, W., Stavrev, K., & Panov, K. 1991, Astron. Nachr., 312, 309

Rots, A. H. 1979, A&A, 80, 255

Saha, A., & Hoessel, J. G. 1991, AJ, 101, 465

Saha, A., Claver, J., & Hoessel, J. G. 2002, AJ, 124, 839

Skillman, E. D., Terlevich, R., Teuben, P., & Van Woerden, H. 1988, A&A, 198, 33

Stil, J. M., & Israel, F. P., 1998, A&A, 337, 64

Stil, J. M., & Israel, F. P., 2002a, A&A, 389, 29

Stil, J. M., & Israel, F. P., 2002b, A&A, 389, 42

Stil, J. M., & Israel, F. P., 2002c, A&A, 392, 473

Strauss, M. A., Huchra, J. P., Davis, M., Yahil, A., Fisher, K. B., & Tonry, J. L. 1992, ApJS, 83, 29.

Tenorio-Tagle, G., Bodenheimer, P., Różyczka, M., Franco, J. 1986, A&A, 170, 107

Tenorio-Tagle, G., Franco, J., Bodenheimer, P., & Różyczka, M. 1987, A&A, 179, 219

Toomre, A., & Toomre, J. 1972, ApJ, 179, 623

Van Zee, L., Westpfahl, D., Haynes, M. P., & Salzer, J. J. 1998, AJ, 115, 1000

Van Zee, L., Skillman, E. D., & Salzer, J. J. 1998, AJ, 116, 1186

Wakker, B. P., & Van Woerden, H. 1991, A&A, 250, 509

Walter, F., & Brinks, E. 2001, AJ, 121, 3016

Warner, P. J., Wright, M. C. H., & Baldwin, J. E. 1973, MNRAS, 163, 163